BINGLEI LI
and
YONGBING LI

Application of grain-based model in simulation of fracture and strength features of brittle rock

Based on the particle flow theory (PFT), the bonded particle model (BPM) and the smooth joint model were combined into a grain-based model, aiming to reveal the micro fracture features of brittle rock. Then, a lattice model was created to reproduce the mechanical properties of the rock, and the samples were under tensile test and uniaxial/triaxial compression under different confining pressures. The tests were conducted to examine the failure mechanism and strength features of the rock. Through the comparison of simulation results and test results, the grain-based model is proved applicable and reliable in the study of mechanical features of brittle rock. During the research, the grain-based model accurately described the crack features of brittle rock in the loading process, and visually reproduced the internal crack development that leads to brittle rock failure. With the ability to simulate brittle material failure of a greater-than-10 compressive-tensile strength ratio, the proposed model can reveal the entire deformation and failure process of brittle rock.

Keywords: Particle flow theory (PFT), brittle rock, grain-based model, crack, lattice structure.

1. Introduction

The destruction of rock is mainly caused by the accumulation of internal cracks. The crack development involves several stages, including production, expansion and penetration. To understand the rock failure mechanism, it is very meaningful to study the crack development process. However, the diversity and complexity of rock have greatly limited the research, making it difficult to fully understand the mechanical properties of the rock.

With the development of rock engineering, rock deformation and failure have been investigated in various means, namely, uniaxial and triaxial tests, acoustic emission test, and stress path loading/unloading test. For instance, reference[1] examines the bending, splitting and uniaxial/triaxial compression features of the granite in the Three Gorges on RMT and MTS rigidity servo testing machines, laying the basis for rational selection of rock breaking and reinforcement tools. Based on the particle flow theory (PFT) and PFC3D, reference[2] establishes rock mass models through the equivalent rock mass technique, and studies the strength and mechanical effect of rock mass; the models can reveal joint distribution features under the fine filtering effect. Reference [3] carries out a direct shear test of rock joints, and discusses the evolution of the joints from both macro and micro angles. Despite the emergence of numerous empirical, numerical and statistical models, it is still difficult to thoroughly explain the rock deformation and failure, disclose the underlying causes of brittle rock rupture, or reproduce the damage process, owing to the non-linear features of the mechanical behaviours of brittle rock [4].

The above problem can be resolved by a novel numerical analysis method called the PFT, which was proposed by P.A. Cundall and O.D.L. Strack based discrete element method. The theory has widely applied to study the basic features of geotechnical materials, the internal rupture of rock mass, the dynamic response and many other fundamental issues. Focusing on the rock mass, numerical simulation models can be created on the PFT[5,6]. Such models analyse the continuous non-linear stress-strain relationship of rock mass, simulate the variation of the medium in the rock mass under the stress environment, and identify particle morphology at each moment based on the particle movement and interaction calculated by displacement and rotation equations. Moreover, these models can reveal the rock fracture mechanism by simulating the particle bonds separated by external forces, which are the key to crack formation and propagation in rock mass.

Among the PFT-based models, the bonded-particle model (BPM) is often used to simulate the meso-mechanics in brittle material fracturing. Reference [7,8] obtains micro mechanical parameters through uniaxial tensile test using the BPM, but the uniaxial tensile strength is so high as to produce a low uniaxial compressive-tensile strength ratio $\sigma ucs/\sigma t$ (the value is usually 4~5), failing to represent the true mechanical features of the brittle rock. The compressive-tensile strength ratio of diorite obtained by the BPM is $(32/7.6) = 4.2$ [9], while the actual compressive-tensile strength ratio of diorite is (193/

10.1)=19.1) [10]. D.O. Potyondy [11] attributed the disparity to the circular or spherical particle units in the model, a far cry from the irregular mineral particles or the structure features of the rock. Therefore, the BPM cannot produce the self-locking effect of rock particles.

To overcome the above problem, this paper combines the PFT-based BPM and a smooth joint model into the grain-based model, calibrates and refines the new model, and uses it to simulate the fracture process of brittle rock with high compressive-tensile strength ratio. It is proved that the proposed model is an effective way to simulate the rupturing of brittle materials with high compressive-tensile strength ratio, e.g. diorite.

2. Construction of grain-based model

The grain-based model is a numerical particle flow model resulted from the merging of a BPM and a smooth joint model[11,13]. The model represents the formation of a rock through the bonding of dense, non-uniform sized circular or spherical particles[14].

2.1 BPM

In the PFT, the movement and interaction between circular particles are simulated by discrete element method. There are mainly three kinds of particle interactions: rigid contact, bonded contact and smooth joint[15]. The bonded contact between two adjacent particles can be simulated by the BPM. The model can be approximated to a small colloidal substance between the two particles (Fig.1).
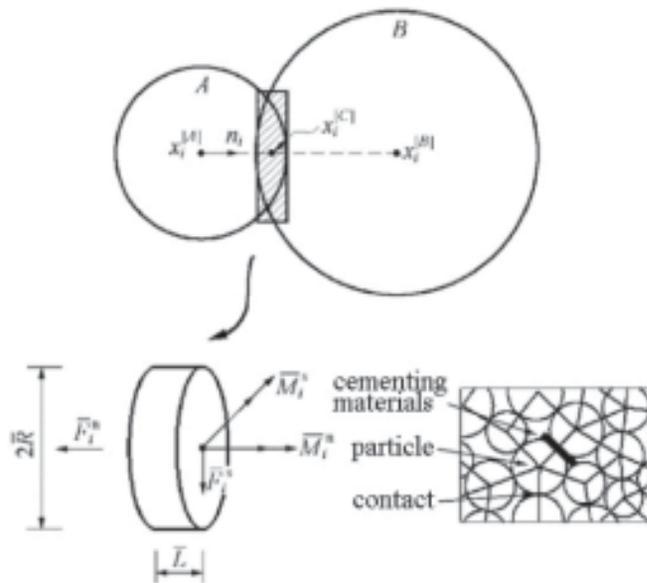
Fig.1 BPM

2.2 SMOOTH JOINT MODEL

As shown in Fig.2, the smooth joint model consists of surface 1, surface 2 and dip angle θ. The direction of the joint plane is expressed by the unit normal vector n_j and the

tangent vector t_j. Both vectors are orthogonal. In the model, particles 1 and 2 are associated with the joint surface.
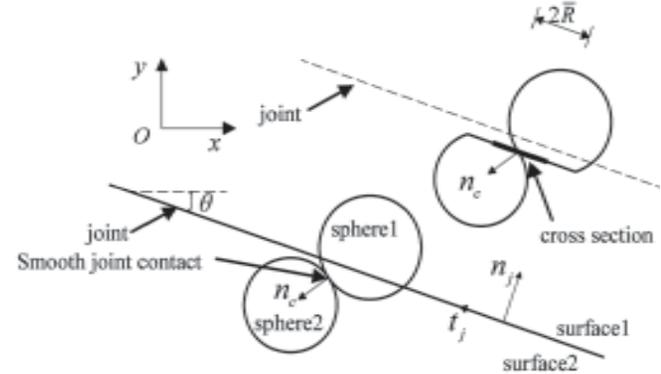
Fig.2 Smooth joint model

Thanks to the circular shape, the smooth joint model can generate random structural faces without considering the contact direction between particles. However, the model allows two contacting particles to slide in parallel along the structural plane, making it difficult to eliminate the bump effect of sliding.

2.3 GRAIN-BASED MODEL

The grain structure is a polygon formed by the gaps between particles. Based on PFC2D, there is no restriction on the surrounding walls, and each particle has at least two contact surfaces. In other words, each contact surface connects two particles and adjoins two gaps. The model is established in the following steps. First, the centre points of the particles were connected to form polygons (Fig.3(a));
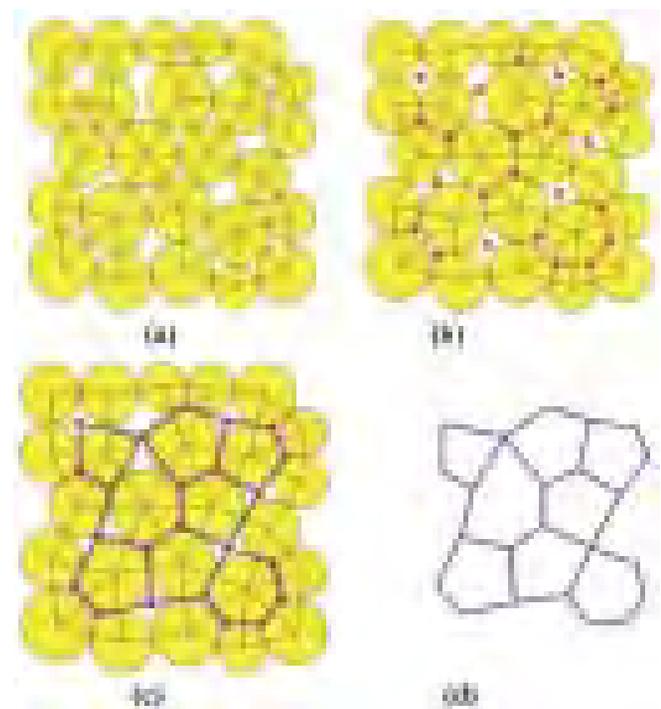
Fig.3 Modelling procedures

second, the centre of each polygon was marked in red (Fig.3(b)); third, the red dots were linked up by lines (Fig.3(c)); fourth, the particles and polygons were deleted to leave the lattice structure (Fig.3(d)).

To close in on the natural state, some synthetic composites of granules (circular/spherical particles or super particles) and binding materials (contact or parallel bonding) were added to the above model. Then, the particle size in the resulting model was refined by replacing the original particle (radius R_0 position X) with the same number of smaller particles (radii R_1 and R_2). The new particles are only in contact with each other with no overlap. The directions and positions of these particles were randomly arranged to maintain the original points of contact.

Without changing the total number of particles, the new radii were determined as follows:

$$R_1^\lambda + R_2^\lambda = R_0^\lambda, \quad \lambda = \begin{cases} 2, 2D \\ 3, 3D \end{cases} \qquad \dots \quad (1)$$

Moreover, the final radius ratio after refinement should not exceed the spherical size ratio (R_{max}/R_{min}) of the base material. The final radius ratio is expressed as:

$$1 \le \frac{R_2}{R_1} \le \beta^{(1/l)} \qquad \dots \quad (2)$$

where $R_1 > R_2$

The R_1 value satisfies both formulas (1) and (2):

$$\left(1 + \beta^{(\lambda/l)}\right)^{-1/\lambda} \le \frac{R_1}{R_0} \le 2^{-1/\lambda} \qquad \dots \quad (3)$$

The radii of the new particles should obey the following constraints:

$$\qquad \dots \quad (4)$$

where α is the refinement parameter valued in the range 0 to 1. If $\alpha = 1$, then $R_1 = R_2$, indicating that the radii of the new particles are equal to the radius of the original particles. In this case, the uniform size of all particles boosts the formation of crystalline material. If $\alpha < 1$, then $R_1 \ne R_2$ indicating that the radii of the new particles are greater than the radius of the original particles. Therefore, the crystalline material should be eliminated at the expense of increasing the size of the new particles.

With all particle sizes being adjusted, the particle density in a specified volume region V should be determined based on the following formula:

$$\rho_b = \rho \left(\frac{V}{\sum_{n_p} V^{(P)}} \right) \qquad \dots \quad (5)$$

where $V(p)$ is the particle volume (p) with n_p particles in the region, assuming that all particles are 2D discs or 3D spheres. This formula applies to materials consisting of circular/spherical particles or super particles.

Then, the lattice was superimposed on the sample particles. Instead of direct super position, further processing is needed to completely fuse the lattice and the sample particles. The particle properties are denoted as ρ, k_n, k_s and μ, and the lattice properties are denoted as ρ, E_c, k_n/k_s and μ. The relationship between particle properties and lattice properties can be explained by the following formulas:

$$k_n = 2tE_c \ (t = 1) \qquad \dots \quad (6)$$

$$k_s = k_n / (k_n / k_s) \qquad \dots \quad (7)$$

If the contact is parallel bonding, then the particle properties should be $\bar{\lambda}, \bar{k}^n, \bar{k}^s, \bar{\sigma}^c, \bar{\tau}_c$ and the lattice properties should be $\bar{k}_s = \bar{k}_n / (\bar{k}_n / \bar{k}_s)$. Then, the relationship between particle properties and lattice properties can be explained by the following formulas:

$$\bar{k}_n = \bar{E}_c / (R_{(A)} + R_{(B)}) \qquad \dots \quad (8)$$

$$\bar{k}_s = \bar{k}_n / (\bar{k}_n / \bar{k}_s) \qquad \dots \quad (9)$$

The refined model is shown in Fig.4
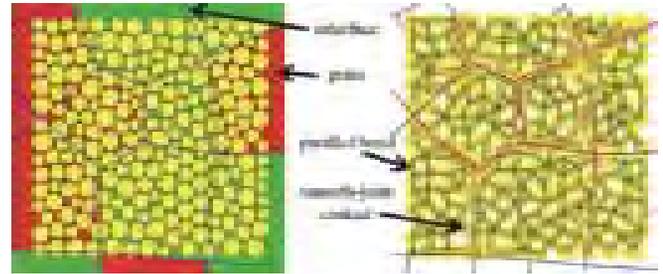
Fig.4 Refined grain structure model

3. Mechanical features of brittle rock and numerical model construction

3.1 Mechanical features of brittle rock

The rupture of rock is a discontinuous event starting with a micro-crack in the interior and at the boundary of the particles [16]. Under the local stress concentration on crack edge, the micro-crack starts to expand and propagate into a macro-crack. The degree of expansion and the number of cracks mainly depend on the microstructure arrangement and density of the grains and cements [17].

One of the most representative experiment on brittle rock mechanical features was conducted by Munoz, H et al[18].

on the granite in the Three Gorges. Under different confining pressures, the rock samples were subject to bending, uniaxial/triaxial compression and Brazilian tension on RMT and MTS servo-controlled testing machines. The test curves and loading point displacements are shown in Fig.5.

(a) Brazilian tension test curve

(b) Uniaxial compression test curve

(c) Triaxial compression test curve under different confining pressure
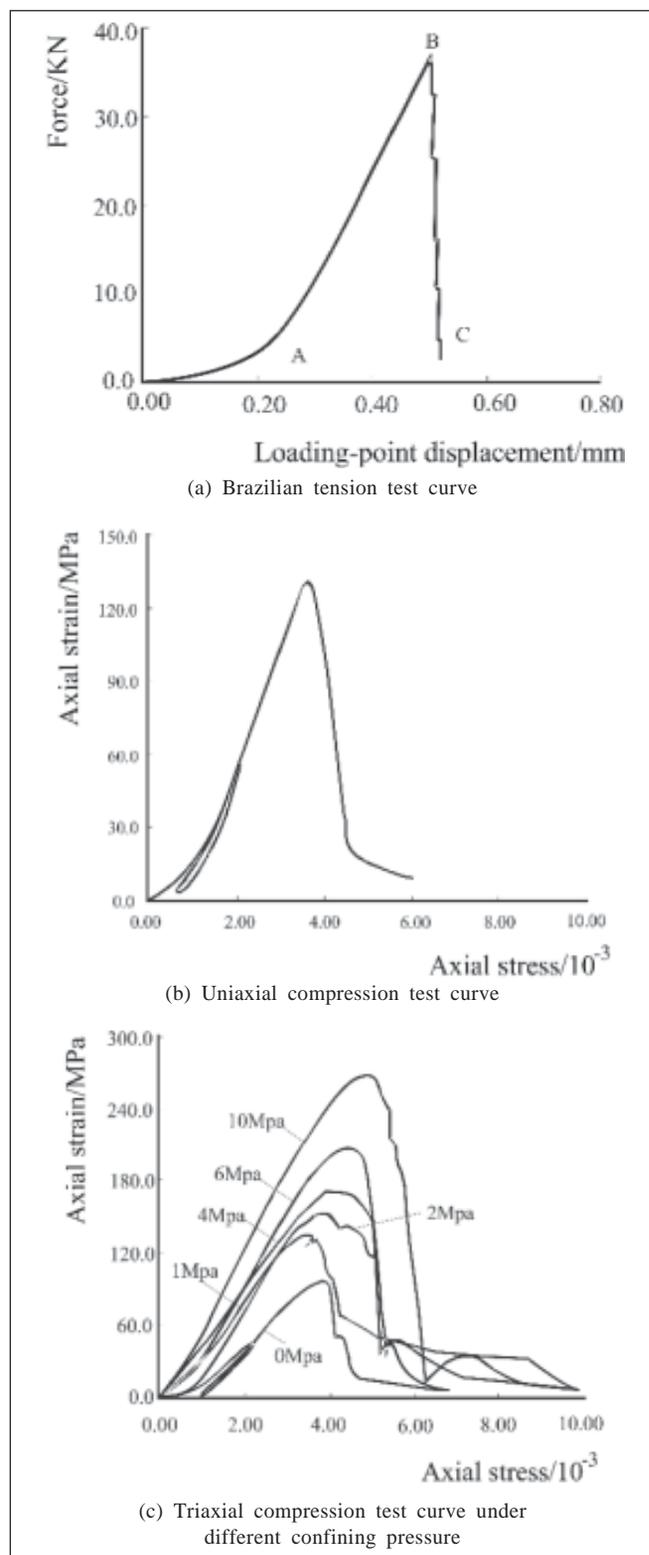
Fig.5 Test curves

In the bending test, 90% of the rock samples had an elastic modulus of 30~70GPa; overall, the elastic modulus averaged at 51.5GPa; the splitting modulus of most rock samples fell in 2~4GPa. In the compression tests, the compressive strength of the rock samples continued to rise; the compressive strength was mainly distributed in 71.3~251.3MPa, with an average compressive strength of 127MPa. Overall, 72% of the rock samples had a compressive strength in 90~150MPa. In the tension test, the tensile strength of the rock samples was measured as 6.18~14.2MPa, and 9.45MPa on average; the compressive-tensile strength ratio ranged between 9.52:1 and 24.27:1, putting the average ratio at 13.4:1. This means the sample rock is a typical high hardness brittle rock.

The detailed fracture mechanism of the granite was acquired by establishing the corresponding meso-structure model based on the granite mechanical properties in [1], and simulating the emergence and expansion of internal cracks with the grain flow simulation programme in grain-based model.

3.2 NUMERICAL MODEL CONSTRUCTION

According to the principle of grain-based model, it is necessary to determine the mechanical parameters of the BPM model and the smooth joint model before the numerical test of the rock mass material. Therefore, a numerical model was created for the particles with the assumed micro-mechanical parameters. Through X-ray diffraction, it is confirmed that main mineral components of the samples are quartz and mica.

For the numerical test, the size of each rock sample is 100mm x 50mm; the radii of circular particles obey Gaussian distribution; the minimum radius of the mineral particles Rmin = 0.25 mm and the maximum radius Rmax = 0.45 mm. The values of the micro-mechanical parameters are listed in Table 1, and the values of the properties of the smooth joints are shown in Table 2.

Fig.6(b) depicts the grain-based grids of the rock sample, where the green and red crystals represent quartz and mica,
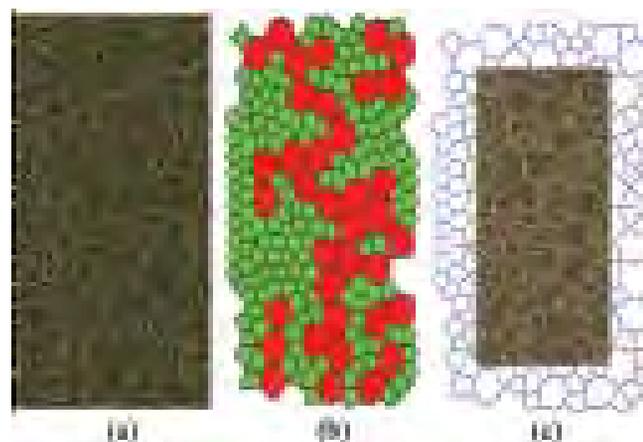
Fig.6 Numerical model construction

TABLE 1: MICRO-MECHANICAL PARAMETERS OF BMP

Attributes	Mineral property value	
	Quartz mineral particles	Mica mineral particles
Parameters related to mineral particles		
Particle density ρ_{ball} [kg/m^3]	3289	2921
Particle elastic modulus E_c [GPa]	100.0	50.0
The ratio of normal to tangential stiffness of particle k_n/k_s	2.5	2.5
Coefficient of friction between particles μ	0.5	0.5
The parameters related to parallel bond		
Parallel bond switch mark $B_{bp\ all}$	0	0
Parallel bond moment contribution factor $\bar{\beta}$	1.0	1.0
Parallel bond radius factor $\bar{\lambda}$	1.0	1.0
Parallel bond elastic modulus $\bar{E}_c$ [GPa]	100.0	50.0
The ratio of normal to tangential stiffness of parallel bond $\bar{k}_n/\bar{k}_s$	2.5	2.5
Parallel bond tensile strength $\bar{\sigma}$ [MPa]	600	400
Parallel bond cohesion $\bar{c}$ [MPa]	1200	800
Parallel bond friction angle $\bar{\phi}$ [degrees]	40	20

TABLE 2: SMOOTH JOINTS PROPERTIES

Attributes	Value	
	Original joint	Newly formed joint
Radius factor $\bar{\lambda}$	1.0	1.0
Normal, shear stiffness $\bar{k}^n, \bar{k}^s$	0.07×inherited	0.07×inherited
Tensile strength σ_c [MPa]	10.1	NA
Cohesion c_b [MPa]	70.0	NA
Friction angle ϕ_b [degrees]	35.0	NA
Friction coefficient μ	0.27	0.27

respectively. Before the superposition of the lattice on the particle model, both the lattice and particles were refined by the refinement algorithm. Finally, a new superposed model was obtained (Fig.6(c)).

4. Numerical analysis of brittle rock features

On the established numerical model, the load was slowly increased until surface cracks appeared on the sample surface. Fig.7 records the distribution of macro-cracks in uniaxial tension, uniaxial compression and triaxial compression tests under different confining pressures.

The results of uniaxial tension test are shown in Fig.7(a). The purple lines represent the failure of the smooth joint model. It can be seen that the cracks were mostly vertical to the axial loading direction, indicating that the sample failure is mainly caused by the bond destruction of adjacent particles.

The results of the uniaxial compression test are shown in Fig.7(b). The purple lines also represent the failure of the smooth joint model. In this test, the tensile cracks emerged at the failure of the smooth joint model on the bond between adjacent particles; these tensile cracks propagated, linked up

(a) Uniaxial tension   (b) Uniaxial compression

(c) Triaxial compression at the confining pressure of 7Mpa   (d) Triaxial compression at the confining pressure of 20Mpa
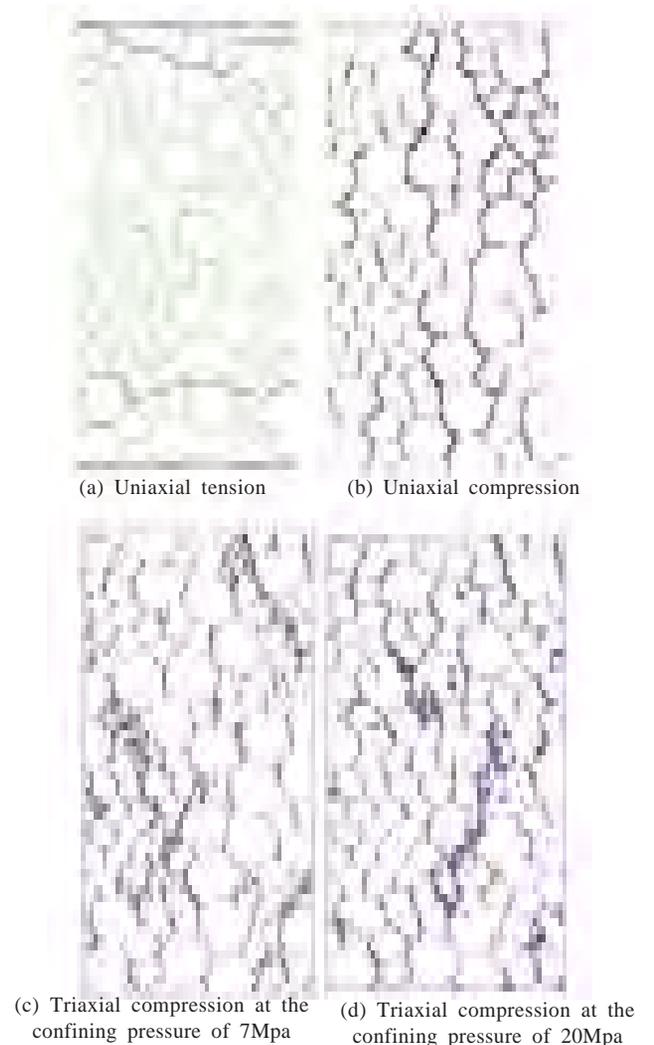
Fig.7 Fracture distributions

Particles number	Elastic modulus /GPa	Poisson's ratio	Confining stress /MPa	Peak stress /MPa	Tensile strength /MPa	Cohesion /MPa	Internal friction angle (o)
	41.05	0.19	0	152.2	7.81	21.7	28.0
	62.19	0.23	1	158.2	7.83	20.9	28.0
6210	68.83	0.27	7	165.8	7.91	22.1	28.0
	65.36	0.27	14	179.6	7.92	20.9	28.0
	68.51	0.29	20	192.1	7.97	21.3	28.0

with each other, forming a macro split crack, and eventually led to the failure of the sample.

Fig.7(c) and (d) are the fracture distribution of the triaxial compression test under different confining pressures. The results are similar to those of uniaxial compression at low confining pressures. However, the increase of confining pressure brought more shear cracks (blue lines in Fig.(d)). With the growing number of shear cracks, a penetrating macro fracture zone formed through the tensile failure and smooth joint failure of the sample.

According to the above analysis, the rock brittleness is positively correlated with the compressive-tensile strength ratio, and the pre- and post- strain difference under axial compression. The greater the rock brittleness, the lower the peak deformation after the axial compression, that is, the greater the ratio of the peak pre-strain and the peak post-strain.

Under external forces, the rock samples underwent three-stage rupturing. First is the crack generation stage. The limited number of cracks in the samples were predominantly tensile cracks. There was basically no shear crack. In the second stage, the tensile and shear cracks increased gradually with the growth of the external load. However, the tensile cracks still far outnumbered shear cracks. The samples exhibited obvious brittle fracture features in the uniaxial test. Further increase in confining pressure led to the multiplication of shear cracks. The shear cracks and tensile cracks almost increased at the same rate before reaching the peak intensity. When the peak intensity was reached, the number of shear cracks surpassed that of tensile cracks (Fig.8).

The failure simulation shows the intergranular, transmission and coupling features of the micro damages on the brittle rock. According to the analysis on the fracture mechanism, the micro-crack features belong to the microstructures of brittle materials under tensile stress. The many randomly distributed micro-cracks are the direct cause of the local tensile stress. With the increase of compressive stress, the number of micro-cracks grew at an increasingly faster speed, leading to gradual growth of the internal energy.

Fig.10(a) shows the stress-strain curve of rock samples under the uniaxial tension test. It can be seen that the strain
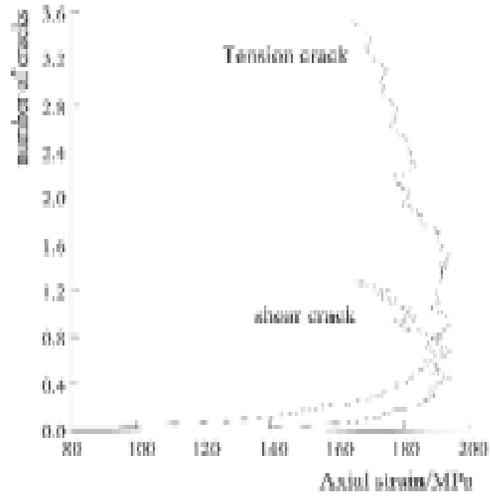
(a) Confining pressure: 7Mpa
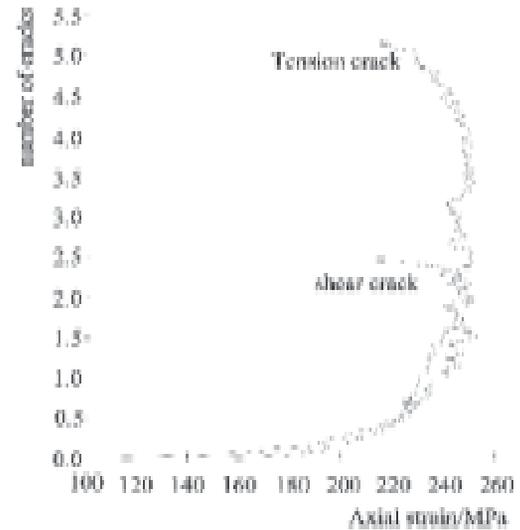
(b) Confining pressure: 20Mpa

Fig.8 Axial stress vs. the number of cracks

declined rapidly with the rising stress at the peak tensile strength. At this moment, the samples carried the features of strong brittle-tensile failure. Fig.10 (b), (c) and (d) respectively show the stress-strain curves of the model in uniaxial and triaxial compression tests under different confining pressures. The arrival of the stress-strain curve at the peak intensity is followed by a short period of strain softening and prominent features of brittle failure.

(c) Confining pressure: 7Mpa

(d) Confining pressure: 20Mpa

Fig.9 Stress-strain curves

(a) Uniaxial tension

(c) Triaxial compression at the confining pressure of 7Mpa

(b) Uniaxial compression

(d) Triaxial compression at the confining pressure of 20Mpa
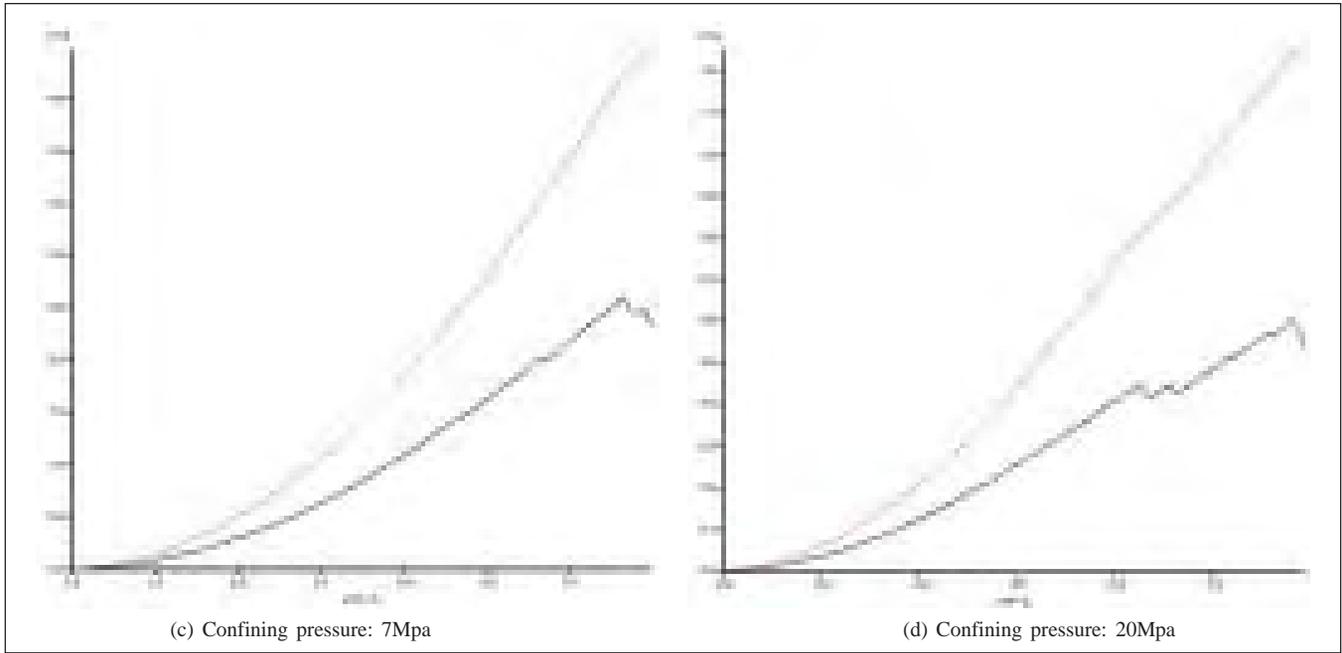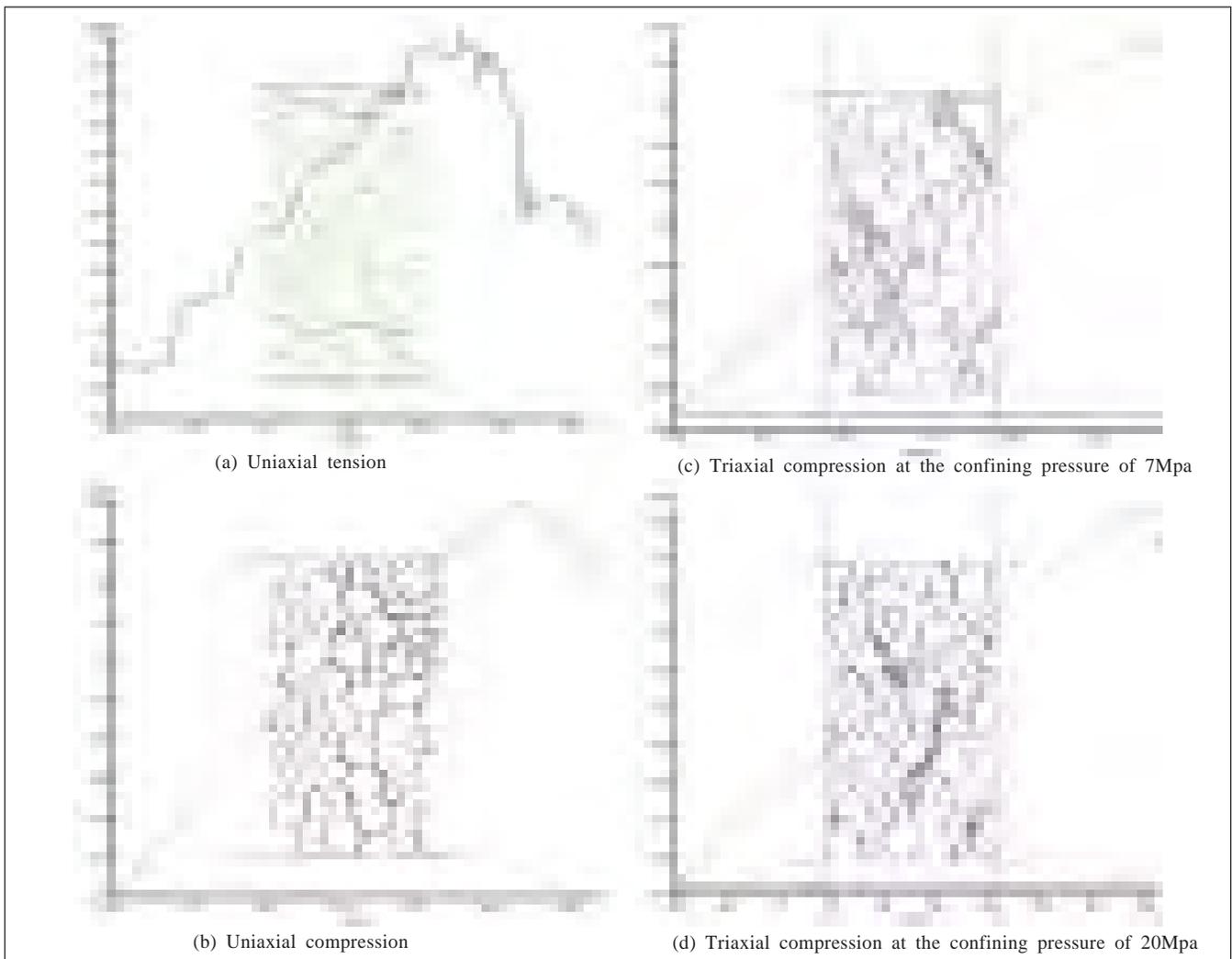
Fig.10 Stress-strain curves

As shown in Table 3, the compressive-tensile strength ratio was minimized at 19.49 and maximized at 24.1. The results are similar to those of Yu Yong's indoor test.

Through the above analysis, it is learned that the non-linear features of the mechanical behaviours of brittle rock is a macro representation of the speed variation in internal micro-crack propagation. The micro-cracks development remains slow in the elastic phase, picks up speed in the plastic phase, and undergoes sudden changes at the point of peak intensity. The numerical simulation accurately reflects the entire process of deformation and failure of brittle rock, especially on the local scale.

5. Conclusions

The grain-based model was constructed to reproduce the mechanical properties of brittle rock. Then, the failure mechanism and strength features of the rock were studied in tensile test, and uniaxial/triaxial compression tests under different confining pressures. Finally, the proposed model was proved applicable and reliable by comparing the simulation results with test results.

During the research, the grain-based model accurately described the crack features of brittle rock in the loading process, and visually reproduced the internal crack development that leads to brittle rock failure. With the ability to simulate brittle material failure of a greater-than-10 compressive-tensile strength ratio, the proposed model can reveal the entire deformation and failure process of brittle rock. Thus, it is possible to replace part of indoor test and in-situ test with the model, laying the basis for unlocking the mechanical properties of brittle rock mass with high compressive-tensile strength ratio.

References

1. Yu, Y. and Wang, T. X. (2004): "Study on relationship between splitting behaviour and elastic modulus of three gorges granite," *Chinese Journal of Rock Mechanics and Engineering*, Vol.19, pp.3258-3261.
2. Wu, S. C., Zhou, Y. and Gao, L. L. (2010): "Application of equivalent rock mass technique to rock mass engineering," *Chinese Journal of Rock Mechanics and Engineering*, Vol.7, pp. 1435-1441.
3. Zhou, Y., Misra, A., Wu, S. C. and Zhang, X. P. (2012): "Macro- and meso-analyses of rock joint direct shear test using particle flow theory," *Chinese Journal of Rock Mechanics and Engineering*, Vol.06, pp. 1245-1256.
4. Guo, S. F., Qi, S. W., Zou, Y. and Zheng, B. W. (2017): "Numerical Studies on the Failure Process of Heterogeneous Brittle Rocks or Rock-Like Materials under Uniaxial Compression," *Materials*, Vol.10, No.4, pp. 1-22.
5. Ghazvinian, E., Diederichs, M. S. and Quey, R. (2014): "3D random Voronoi grain-based models for simulation of brittle rock damage and fabric-guided micro-fracturing," *Journal of Rock Mechanics and Geotechnical Engineering*, Vol.06, No.06, pp.506-521.
6. Li, Y., Li, Z. and Xu, T. J. (2013): "Research of Brittle Shear Failure Strength of Rock Materials," *Applied Mechanics and Materials*, Vol.454, pp.125-128.
7. Heap, M. J., Russell, J. K. and Kennedy, L. A. (2016): "Mechanical behaviour of dacite from Mount St. Helens (USA): A link between porosity and lava dome extrusion mechanism (dome or spine)," *Journal of Volcanology and Geothermal Research*, Vol.328, pp.159-177.
8. Xiang, W. F. and Zhou, C. B. (2005): "The research progress of the fractured rock mass," *Chinese Journal of Rock Mechanics and Engineering*,Vol.24(add 2), pp.5686-5692.
9. Momber, A. W. (2016): "The response of geo-materials to high-speed liquid drop impact," *International Journal of Impact Engineering*, Vol.89, pp.83-101.
10. Zhu, H. C., Patrick, A. and Zhong, H. Y. (2005): "Numerical calculation method and application of jointing rock mass: engineering application," *Chinese Journal of Rock Mechanics and Engineering*, Vol.24(1), pp.89-96.
11. Liu, Z. C. (2009): "Research on Mechanics Properties of the Brittle Rock with Triaxial Unloading Experiment," *Journal of North China Institute of Science and Technology*, Vol.6(3), pp.10-12.
12. Huang, D. and Li, X. Q. (2017): "Numerical simulation research on characteristic strength of marble based on development of microcrack," *Rock and Soil Mechanics*, Vol.38, No.1, pp.253-262.
13. Zhou, Y., Gao, Y. T., Wu, S. C., Yan, Q. and Sun, H. (2015): "An equivalent crystal model for mesoscopic behaviour of rock," *Chinese Journal of Rock Mechanics and Engineering*, Vol.3, pp.511-519.
14. Gao, F. Q., Doug, S. and Davide, E. (2016): "Numerical simulation of microstructure of brittle rock using a grain-breakable distinct element grain-based model," *Computers and Geotechnics*, Vol.78, pp 203-217.
15. Li, Y. W., Jia, D., Rui, Z. H., Peng, J. Y., Fu, C. K. and Zhang, J. (2017): "Evaluation method of rock brittleness based on statistical constitutive relations for rock damage," *Journal of Petroleum Science and Engineering*, vol.153, pp 123-132.
16. Park, J. W., Park, C., Song, J. W., Park, E. S. and Song, J. J. (2017): "Polygonal grain-based distinct element modeling for mechanical behavior of brittle rock," *International Journal for Numerical and Analytical Methods in Geomechanics*, Vol.41, No.6, pp.880-898.
17. Park, J. W., Park, C., Song, J. W., Park, E. S. and Song, J. J. (2017): "Erratum to the 'polygonal grain-based distinct element modeling for mechanical behavior of brittle rock'," *International Journal for Numerical and Analytical Methods in Geomechanics*, Vol.41, No.13, pp.1474.
18. Munoz, H., Taheri, A. and Chanda, E. (2016): "Fracture Energy-Based Brittleness Index Development and Brittleness Quantification by Pre-peak Strength Parameters in Rock Uniaxial Compression," *Rock Mechanics & Rock Engineering*, Vol.49, No.12, pp.4587-4606.